CCS Chemistry

RESEARCH ARTICLE

Received: Aug. 19, 2023 | Accepted: Sept. 19, 2023 | Published: Oct. 26, 2023

Enhanced Photocatalytic CO_2 Reduction via Linkage Substitution in Porphyrinic Covalent Organic Frameworks

Suleman Suleman, Kang Sun, Yiming Zhao, Xinyu Guan, Zhongyuan Lin, Zheng Meng* & Hai-Long Jiang*

Department of Chemistry, University of Science and Technology of China, Hefei, Anhui 230026

*Corresponding authors: zhengmeng@ustc.edu.cn; jianglab@ustc.edu.cn

Cite this: *CCS Chem*. **2024**, 6, 1689–1697
DOI: 10.31635/ccschem.023.202303319

A catalytic performance is greatly impacted by the microenvironment surrounding the catalytic centers. However, efforts to modify the microenvironment are primarily directed towards the first coordination spheres, while controlling the secondary coordination spheres is entirely restricted. In this work, a series of porphyrin-based covalent organic frameworks (COFs) with distinct linkage were rationally designed to investigate the structure–property relationship between the secondary coordination spheres of catalytic centers and CO_2 photoreduction. The secondary coordination spheres of COFs could be changed readily by manipulating the organic linkage. In photocatalytic CO_2 reduction, the COF with β-ketoenamine as the linkage (NiPor-BDOB) exhibited superior activity, selectivity, and stability over its imine-linked counterpart (NiPor-BDA). Experiments and theoretical calculations indicated that the distinct secondary coordination sphere resulted in an electronic density change of Ni centers, leading to enhanced photocatalytic performances. This study highlights the significance of controlling the secondary coordination sphere around the active site.

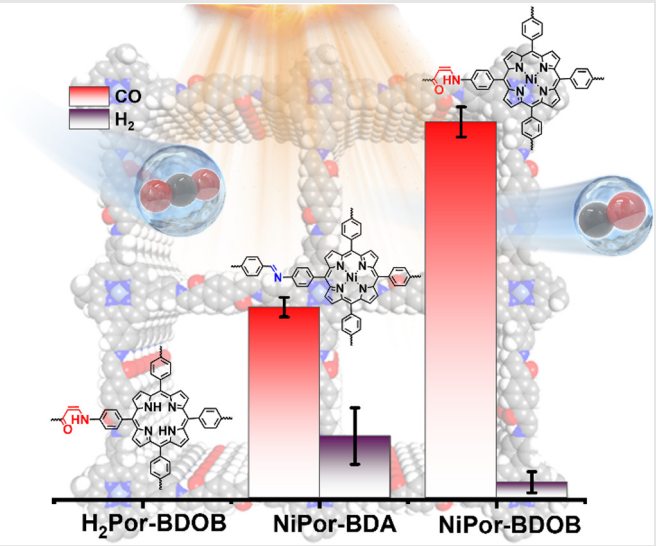

Keywords: covalent organic frameworks, linkage substitution, photocatalysis, CO_2 reduction, activity, selectivity

Introduction

Photocatalytic CO_2 reduction offers an appealing pathway for producing fuels and valuable chemicals, capitalizing on renewable and abundant solar energy for long-term CO_2 utilization.[1,2] The ultimate objective is to combine the reductive process of CO_2 with a complementary oxidative process such as water oxidation to establish a carbon-neutral artificial photosynthesis cycle.[3,4] Before achieving this ultimate objective, numerous fundamental scientific obstacles were associated with the development of systems that balance selectivity,

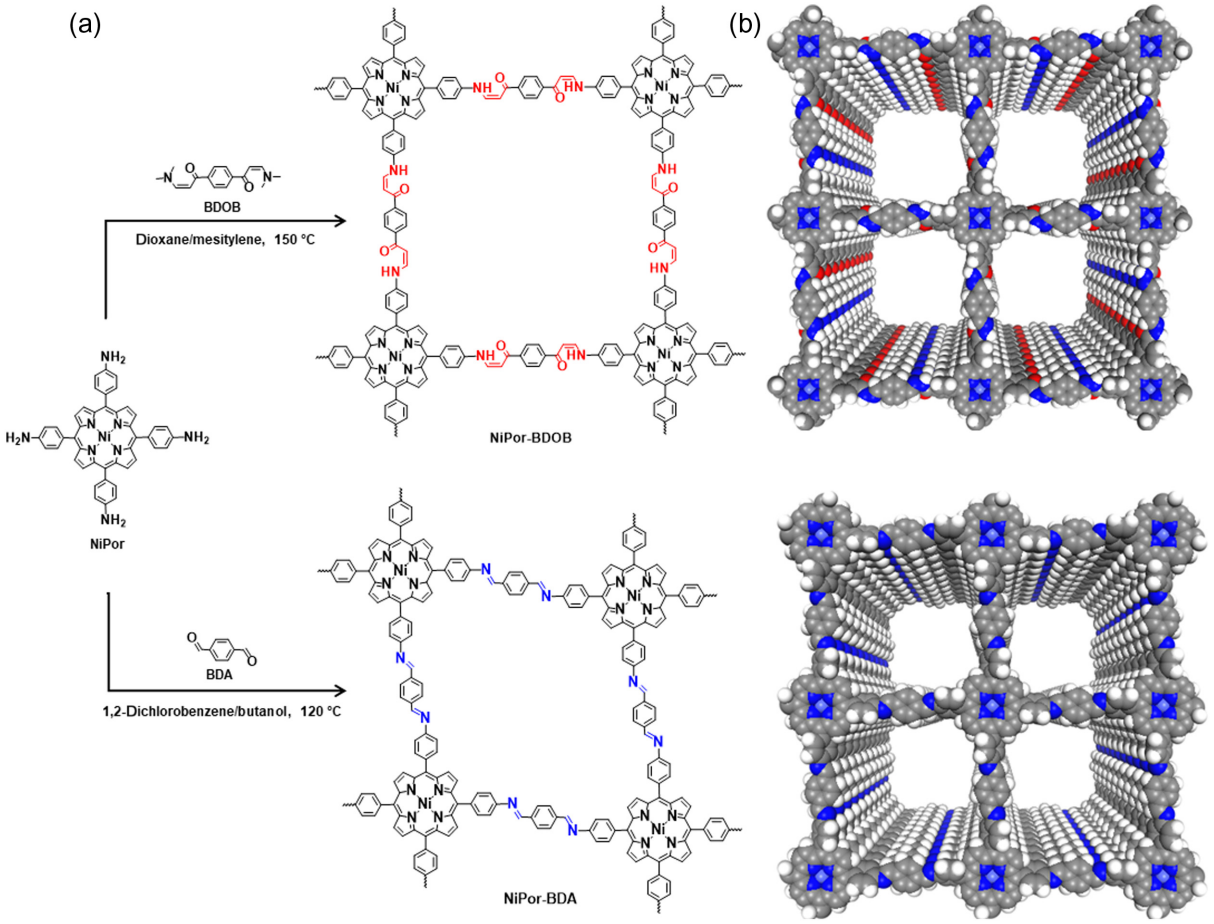

Figure 1 | *(a) Synthetic scheme of NiPor-BDOB and NiPor-BDA. (b) The optimized structural models of NiPor-BDOB and NiPor-BDA.*

efficiency, and stability. However, current systems for light-induced conversion of CO_2 to reduced carbon products suffer from low activity and poor selectivity.[5–7] Therefore, developing photocatalysts with high activity and selectivity for CO_2 photoreduction is highly desirable.

In the photocatalytic process, catalytic sites are responsible for CO_2 adsorption and activation. The meticulous arrangement of electronic configurations in catalytic sites profoundly influences the efficiency and specificity of photocatalytic CO_2 reactions.[8] Many strategies have been developed to modulate the electronic structures of catalytic sites; among them, regulating the coordination spheres surrounding catalytic centers is one of the most direct methods.[9,10] Most strategies for the modulation of coordination spheres focus on the first coordination spheres. However, the secondary coordination spheres around catalytic sites, which also significantly influence catalytic performance, have been largely overlooked. Although some strategies have been developed to modulate secondary coordination spheres in molecular catalysts,[11] it remains challenging and rare for heterogeneous catalysts due to their rigid structures. Therefore, it is highly demandable to construct photocatalysts that possess atomically precise and highly designable structures for secondary coordination spheres' modulation.

Covalent organic frameworks (COFs) are a unique class of crystalline porous polymers built by linking molecular organic building blocks with strong covalent bonds.[12–15] The periodic, well-defined, and designable architectures of COFs are highly desirable for precise control of their characteristics and function in selective and effective photocatalytic CO_2 reduction.[16–19] Rationally designing the building units (linkers) and the bonds that form between these units can effectively influence their photocatalytic performance while maintaining the topological structure of the COFs, a prerequisite to investigating the structure-property relationship in photocatalysis. The exploration of linkers with different symmetries,[20,21] lengths,[22,23] and functional groups[24–27] has been extensively studied in photocatalysis. However, the impact of linkages remains relatively unexplored and poorly understood, despite their potential significance in influencing stability, light absorption, charge separation, and other key factors of COFs. In addition, the focus

DOI: 10.31635/ccschem.023.202303319
Citation: *CCS Chem.* **2024**, 6, 1689–1697
Link to VoR: https://doi.org/10.31635/ccschem.023.202303319

of research in photocatalysis is primarily on imine and its derivatives-based linkages. However, the moderate stability of most imine-based COFs, especially when exposed to prolonged light, hampers their more comprehensive application.[28–30] Considering these factors, it is hypothesized that COFs could serve as promising candidates for precise regulation of the secondary coordination spheres around the catalytic sites for enhanced CO_2 photoreduction.[31]

In this work, we constructed two types of porphyrin-based COFs, NiPor-BDOB and NiPor-BDA, with the latter referred to as COF-366(Ni);[32] synthesized by linking nickel porphyrin (NiPor) units (Supporting Information Scheme S1) with 1,4-bis(3-dimethylamino-1-oxopropyl) benzene (BDOB) (Supporting Information Scheme S2) and 1,4-benzenedicarboxaldehyde (BDA) as linker, respectively, for photocatalytic CO_2 reductions (Figure 1a, b). Compared to imine-linked NiPor-BDA, NiPor-BDOB exhibits a significant 50% improvement in CO_2 photoreduction activity and a 77% enhancement in selectivity. Furthermore, thanks to the superior stability of the β-ketoenamine linkage; NiPor-BDOB demonstrated improved reaction stability and ultrahigh resistance to harsh acid/base conditions compared to imine-linked NiPor-BDA. Experimental characterizations combined with theoretical calculations indicate that the linkage modulations regulate the electronic density of Ni sites and the charge-transfer dynamics, resulting in different activation barriers for forming key intermediates in CO_2 reduction, leading to discriminative catalytic activity. This work shows that linkage-based modulation in COFs can serve as a powerful means for carefully crafting and adjusting the coordination microenvironment of catalytic metal sites for high performance in photocatalytic CO_2 reduction.

Experimental Methods

Synthesis of H_2Por-BDOB

To a Pyrex tube metal-free porphyrin (H_2Por, 13.5 mg, 0.02 mmol), BDOB (10.9 mg, 0.04 mmol), benzyl alcohol (0.5 mL), *o*-dichlorobenzene (*o*-DCB), and 6 M acetic acid (0.1 mL) were added. Then the solution mixture was sonicated for 5 min and frozen at 77 K (liquid N_2 bath). Afterward, the tube was evacuated to an internal pressure of 50 mTorr and sealed off. The reaction proceeded in the oven at 120 °C for 72 h. After cooling to room temperature, the crude H_2Por-BDOB product was washed with tetrahydrofuran (THF), acetone, and methanol. Finally, the product was treated with supercritical CO_2 to yield the activated COF. A similar synthetic procedure used for H_2Por-BDOB was also employed in the synthesis of NiPor-BDOB (Supporting Information Figure S1), as described below. Note that the NiPor-BDOB obtained by this procedure was not highly crystalline.

Synthesis of NiPor-BDOB

To a Pyrex tube NiPor (14.5 mg, 0.02 mmol) BDOB (10.9 mg, 0.04 mmol), dioxane (0.5 mL), mesitylene (0.5 mL), and acetic acid (0.1 mL) were added, sonicated for 5 min. Then the tube mixture was frozen at 77 K (liquid N_2 bath). Afterward, the tube was evacuated to an internal pressure of 50 mTorr and sealed off. The reaction proceeded in the oven at 150 °C for 72 h. After cooling to room temperature, the product was washed with THF, acetone, and methanol. Finally, the crude NiPor-BDOB product was treated with supercritical CO_2 to yield the activated COF.

Photocatalytic CO_2 reduction experiments

The photocatalytic CO_2 reduction experiments were conducted at room temperature in a 160 mL photoreactor (Beijing Perfect Light Technology Co., Ltd., Beijing, China). A mixture of the H_2Por-BDOB, NiPor-BDOB, or NiPor-BDA catalyst (5 mg), photosensitizer $[Ru(bpy)_3]Cl_2{\cdot}6H_2O$ (5 mg), triethylamine (TEA, 0.7 mL), acetonitrile (CH_3CN, 8.8 mL), and deionized water (H_2O, 1.5 mL) was added into the photoreactor. After a homogeneous solution with sonication, the reactor was degassed with CO_2 for 15 min to remove the air. A 300 W Xe lamp irradiated the reaction system. The evaluation of CO gas generation was determined by gas chromatography, in which 200 μL of the headspace was injected into the gas chromatography (Shimadzu GC-2014, assembled in China, Japan brand, argon as carrier gas). The products were quantified by gas chromatography achieved using a reference calibration plot, generated using internal hydrogen and CO standards. During the recycling experiments, the solution collected after the reaction was centrifuged and washed twice with acetonitrile. The catalyst was reused in the next cycle with the addition of $[Ru(bpy)_3]Cl_2{\cdot}6H_2O$ under the same reaction conditions.

Results and Discussions

Synthesis and characterizations

The COF NiPor-BDOB was synthesized using solvothermal conditions in sealed ampules via the condensation of BDOB with NiPor. The optimal crystallinity of NiPor-BDOB was achieved when a mixed solvent of dioxane and mesitylene (v/v = 5:5) was used at 150 °C. For the elucidation of the role of Ni sites in the β-ketoenamine linked COF NiPor-BDOB in photocatalytic CO_2 reduction, the COF H_2Por-BDOB was also made by reacting H_2Por with BDOB in a mixture of benzyl alcohol and *o*-DCB (v/v = 5:5) at 120 °C. The imine-linked COF NiPor-BDA was synthesized by condensation between NiPor with BDA, following a previously reported method (see Supporting Information for details).[33]

DOI: 10.31635/ccschem.023.202303319
Citation: *CCS Chem.* **2024**, 6, 1689–1697
Link to VoR: https://doi.org/10.31635/ccschem.023.202303319

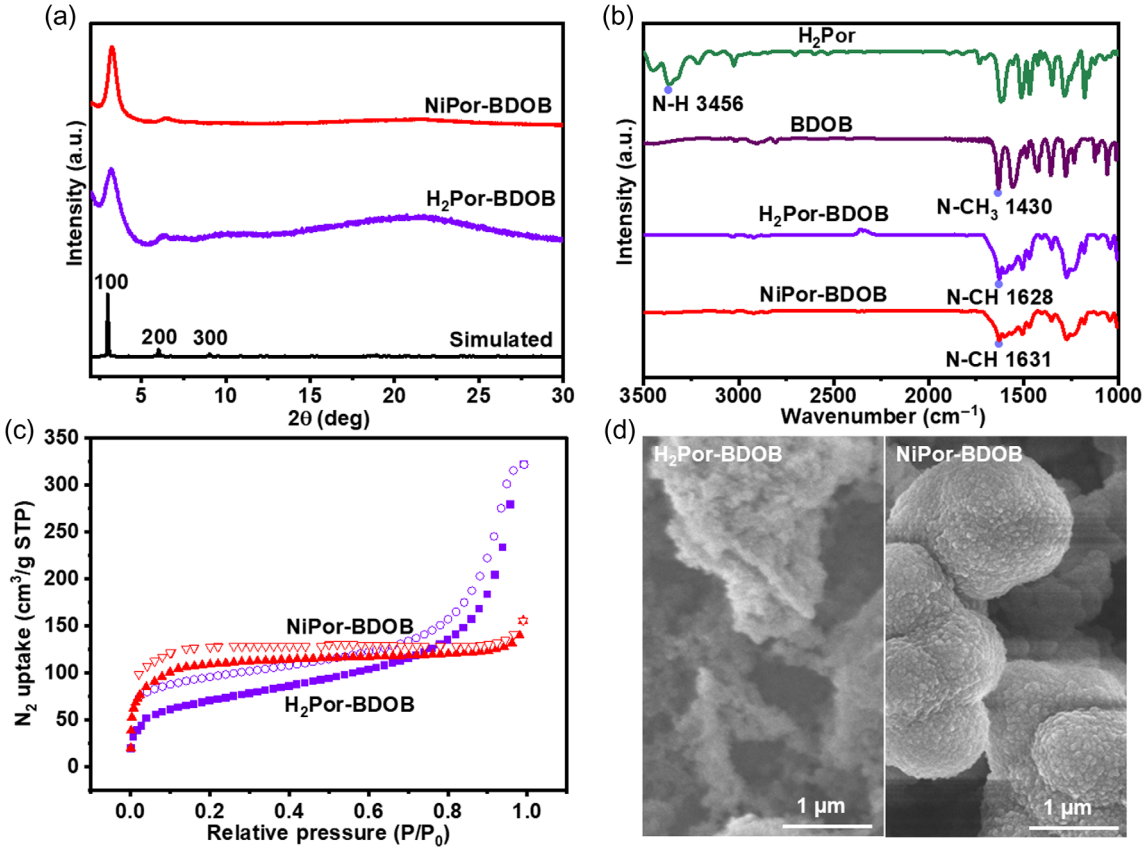

Figure 2 | *(a) Simulated and experimental PXRD pattern of H_2Por-BDOB and NiPor-BDOB. (b) FT-IR spectra of H_2Por-BDOB and NiPor-BDOB along with starting reagents. (c) Nitrogen adsorption–desorption isotherm for H_2Por-BDOB and NiPor-BDOB (d). SEM images of H_2Por-BDOB and NiPor-BDOB.*

The successful construction of the β-ketoenamine-linked COFs was confirmed by powder X-ray diffraction (PXRD). The PXRD patterns of H_2Por-BDOB and NiPor-BDOB showed prominent peaks at 2.9°, 5.8°, and 8.7°, assigned to diffractions of (100), (200), and (300) planes. Furthermore, the predicted PXRD patterns aligned with the experimental results, along with low refinement agreement factors for H_2Por-BDOB and NiPor-BDOB (Figure 2a and Supporting Information Figure S2). The absence of residual peaks of the starting monomers and other species suggested a good phase purity of H_2Por-BDOB and NiPor-BDOB. The PXRD patterns of the COFs closely matched with eclipsed packing mode of the simulated PXRD patterns. The presence of nickel within the coordinating porphyrin units was verified by solid-state ultraviolet–visible (UV–vis) spectroscopy (Supporting Information Figure S3) and inductively coupled plasma atomic emission spectrometer (ICP-AES; Supporting Information Table S1). Fourier transform infrared (FT-IR) spectroscopy verified the disappearance of the N-CH_3 bond of BDOB at 1430 cm^{-1} and the formation of N-CH vibrations of H_2Por-BDOB and NiPor-BDOB at 1628 cm^{-1}, implying the successful construction of β-ketoenamine moiety (Figure 2b).[34] In addition, a peak appeared at 145.13 ppm in solid-state cross-polarization/magic-angle-spinning (CP/MAS) ^{13}C NMR spectroscopy, supporting the presence of 2-ketoenamine in NiPor-BDOB (Supporting Information Figure S4).[34] The Brunauer–Emmett–Teller (BET) surface areas of H_2Por-BDOB and NiPor-BDOB are 250.4 and 425.3 m^2/g, respectively (Figure 2c and Supporting Information Figures S5 and S6). Scanning electron microscopy (SEM) revealed that H_2Por-BDOB showed staggered branches, and NiPor-BDOB contained a spherical aggregation of irregular nanometer-sized particles (Figure 2d). As a control, NiPor-BDA with imine linkages was prepared; its characterizations, including PXRD and FT-IR, matched well with the reported results (Supporting Information Figures S7 and S8).[35] The BET surface area of NiPor-BDA was 1117.9 m^2/g (Supporting Information Figure S9).

Encouraged by the successful characterizations, we investigated the stability of NiPor-BDOB and NiPor-BDA by immersing the COFs in 20 M NaOH, 1 M HCl, 3 M HCl, and 6 M HCl solutions for 12 h. The NiPor-BDOB maintained relatively good crystallinity as verified by PXRD (Supporting Information Figure S10), which revealed superior chemical stability of NiPor-BDOB COF due to the

DOI: 10.31635/ccschem.023.202303319
Citation: *CCS Chem.* **2024**, 6, 1689–1697
Link to VoR: https://doi.org/10.31635/ccschem.023.202303319

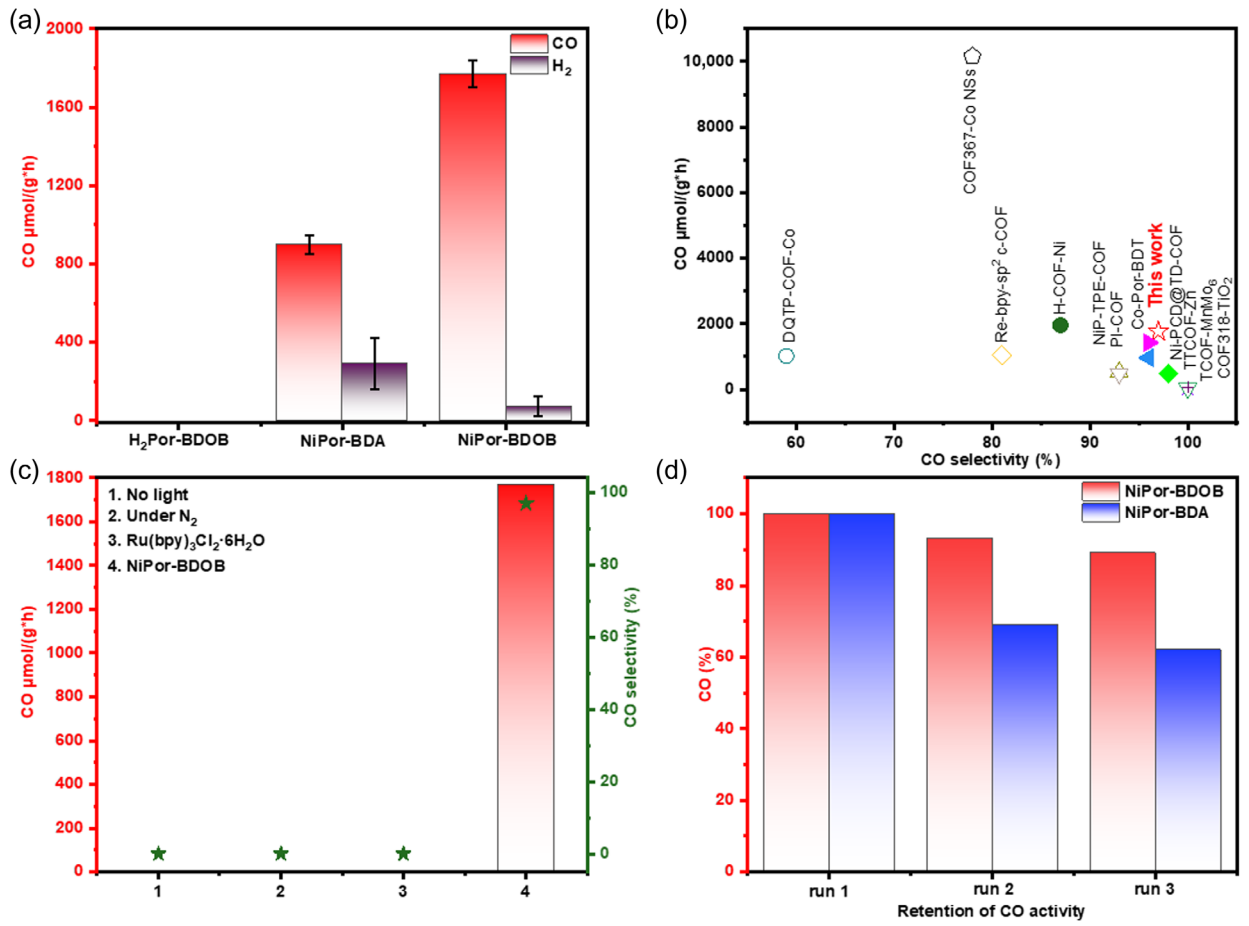

Figure 3 | *(a) CO generation rate with three COFs after 1 h of reaction. (b) Comparison of the activity and selectivity of NiPor-BDOB with the previously reported photocatalytic CO_2 reductions. (c) The efficiency of photocatalytic CO_2 reduction under a range of diverse reaction conditions. (d) Reusability test of NiPor-BDOB and NiPor-BDA.*

stable β-ketoenamine linkage.[36] In sharp contrast, the crystallinity of NiPor-BDA diminished significantly under the above conditions (Supporting Information Figure S11).

Photocatalytic CO_2 reduction

The photocatalytic reduction of CO_2 was conducted in a suspension of the COF catalysts (5.0 mg), $[Ru(bpy)_3]Cl_2$ (5.0 mg), acetonitrile (MeCN, 8.8 mL), water (1.5 mL), and TEA (0.7 mL), saturated with CO_2 at ambient temperature under light irradiation with a Xe lamp (see Supporting Information for details). When NiPor-BDA was used as a catalyst under optimal conditions, the production rates for CO and H_2 were 898 μmol/(g_{cat} h) and 291 μmol/(g_{cat} h), respectively, resulting in a 75% selectivity for CO (Figure 3a). Under the same conditions, NiPor-BDOB exhibited CO and H_2 evolution rates of 1770 and 40 μmol/(g_{cat} h), respectively, with a remarkable 97% selectivity for CO. In terms of both activity and selectivity, NiPor-BDOB stood out as one of the best examples of COFs that integrated high activity and selectivity (Figure 3b and Supporting Information Table S2). In the absence of both light and NiPor-BDOB, no CO product was detected (Figure 3c), highlighting the paramount importance of light and the photocatalyst. In addition, using H_2Por-BDOB (Supporting Information Table S3) also gave no CO product, indicating that Ni sites in NiPor-BDOB (Supporting Information Table S4) likely act as the catalytic center for CO_2 reduction. To trace the source of CO, isotope-labeled experiments using $^{13}CO_2$ instead of $^{12}CO_2$ were conducted under optimized conditions (Supporting Information Figure S12). The result undoubtedly proved that the CO originated from the process of CO_2 reduction. Furthermore, the recyclability of NiPor-BDOB was examined by running three successive photocatalytic cycles under identical conditions. Only an 11% drop in activity was observed for NiPor-BDOB, suggesting its good reusability (Figure 3d). The PXRD verified the structural integrity and crystallinity of the NiPor-BDOB after the photocatalytic test (Supporting Information Figure S13). In contrast, the activity of NiPor-BDA (Supporting Information Table S5) after three photocatalytic cycles, dropped from 100 to 62%. This comparison demonstrated the

DOI: 10.31635/ccschem.023.202303319
Citation: *CCS Chem.* **2024**, 6, 1689–1697
Link to VoR: https://doi.org/10.31635/ccschem.023.202303319

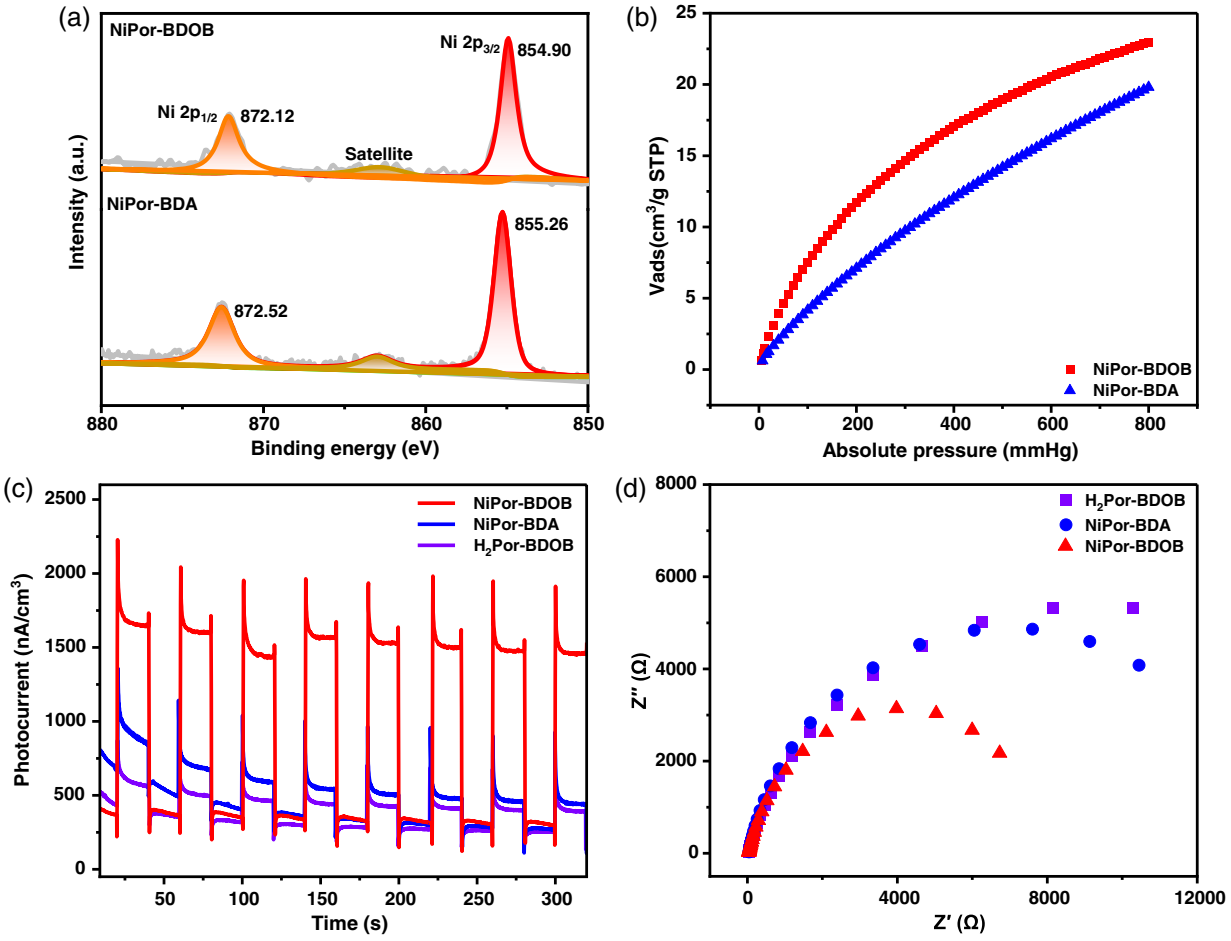

Figure 4 | *(a) XPS Ni 2p spectra of NiPor-BDOB and NiPor-BDA. (b) CO_2 adsorption spectra of NiPor-BDOB and NiPor-BDA at 298 K. (c) Photocurrent responses and (d) EIS Nyquist plots of NiPor-BDOB, NiPor-BDA, and H_2Por-BDOB.*

good durability of the NiPor-BDOB for photocatalysis, ascribed to the robust β-ketoenamine linkage.

Mechanistic studies

Encouraged by the above analysis, we conducted various experiments coupled with theoretical calculations to further explore the underlying mechanism for the distinct photocatalytic CO_2 reduction performance of the COFs modulated by the linkage. First, we investigated the charge transfer paths in photocatalysis. The bandgaps of two Ni-based COFs, NiPor-BDOB and NiPor-BDA, were analyzed using UV–vis diffuse reflectance spectra (Supporting Information Figures S14 and S15). Based on the Tauc plot analysis, the E_g of NiPor-BDOB and NiPor-BDA were calculated at 1.83 and 1.86 eV, respectively (Supporting Information Figures S16 and S17). Furthermore, Mott–Schottky measurements have been carried out at three different frequencies to determine the conduction band (CB) positions (Supporting Information Figures S16 and S17). A positive slope was observed when examining the relationship between C^{2-} values and applied potentials, indicating a typical *n*-type semiconductor behavior.[37] The calculated conduction band minimums (CBMs) of NiPor-BDOB and NiPor-BDA were −0.59 and −0.96 V versus normal hydrogen electrode (NHE), respectively, lower than the redox potential of CO_2 to CO (−0.53 V vs NHE at pH 7) and higher than the potential (−1.31 V vs NHE) of the $[Ru(bpy)_3]Cl_2$. This finding indicated that the excited electrons could transfer from $[Ru(bpy)_3]Cl_2$ to COF and further drive CO_2 reduction. Furthermore, NiPor-BDA had a higher CB position than NiPor-BDOB, indicating that NiPor-BDOB was thermodynamically more favorable for CO_2 reduction. This result suggested that the difference in activity between the two COFs did not originate from the different band structures.

Furthermore, the electronic states of Ni sites in NiPor-BDOB and NiPor-BDA were also investigated by X-ray photoelectron spectroscopy (XPS). The XPS showed that the binding energy of Ni $2p_{3/2}$ for NiPor-BDOB appeared at 854.90 eV, which was smaller than 855.26 eV for NiPor-BDA (Figure 4a). The lower Ni $2p_{3/2}$ binding energy of NiPor-BDOB suggested that the electronic

DOI: 10.31635/ccschem.023.202303319
Citation: *CCS Chem.* **2024**, 6, 1689–1697
Link to VoR: https://doi.org/10.31635/ccschem.023.202303319

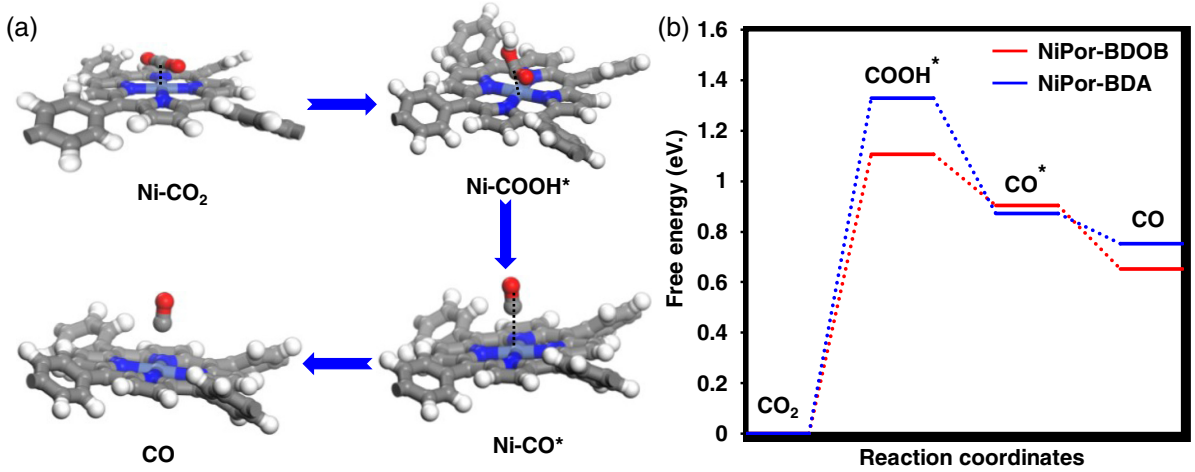

Figure 5 | *(a) The free energy profiles describe the CO_2 photoreduction to CO over NiPor-BDOB and NiPor-BDA. * Represents active centers during the photocatalytic CO_2 reduction. (b) Illustrations of the reaction path in the photocatalytic reduction of CO_2 by NiPor-BDOB.*

density of Ni sites was more negative. The difference in the electronic state of the Ni active center of the two COFs should affect the adsorption of CO_2 molecules on the catalytic sites, which is the first step for CO_2 photoreduction. The CO_2 absorption experiments were further conducted on NiPor-BDOB and NiPor-BDA. The results showed that NiPor-BDOB exhibited a CO_2 adsorption capacity of 23 $cm^3\ g^{-1}$ at 298 K (1 bar), which was 28% higher (18 $cm^3\ g^{-1}$) than that of NiPor-BDA. This demonstrated that the distinct secondary coordination spheres around Ni sites indeed resulted in a discrepancy in CO_2 adsorption capacity. The enhanced CO_2 adsorption capacity in NiPor-BDOB might be beneficial to the CO_2 reduction performance by improving CO_2 preconcentration around active sites and adsorption on active sites (Figure 4b).[38–40]

Given the significantly greater photocatalytic activity observed in NiPor-BDOB compared to NiPor-BDA, we posited that the efficiency of photoinduced electron-hole (e^-/h^+) separation played a critical role.[41,42] Photocurrent measurements revealed that NiPor-BDOB generated a much higher photocurrent response than NiPor-BDA, indicating that the former exhibited a more effective separation of e^-/h^+ pairs (Figure 4c). Further analysis through electrochemical impedance spectroscopy (EIS) resulted in NiPor-BDOB demonstrating a smaller radius than NiPor-BDA (Figure 4d). This result suggested a lower charge-transfer resistance in NiPor-BDOB, indicating possible faster electron transfer from photosensitizers to COF for enhanced CO_2 reduction activity. This finding indicated that NiPor-BDOB exhibited higher charge-separation efficiency compared to NiPor-BDA, despite the fact that both COFs shared similar building blocks yet different linkages. The higher charge-separation efficiency might have led to improved electron transfer efficiency in the photocatalytic CO_2 reduction.[43,44]

To further investigate the origin of the difference in CO_2 photoreduction performance between NiPor-BDOB and NiPor-BDA, density functional theory (DFT) calculations were conducted. We considered four consecutive reaction steps for the CO_2 reduction reaction on the metal catalytically active site (Figure 5a). The free energy calculation showed that the rate-determining step was the formation of *COOH. The free energy for the formation of *COOH intermediate step on the Ni site of NiPor-BDOB active sites was 1.10 eV. In contrast, NiPor-BDA showed a lower free energy activation barrier of 1.32 eV for the formation of *COOH (Figure 5b). Therefore, the Ni site in NiPor-BDOB was identified as a more favorable active site for CO_2 reduction reaction based on thermodynamics analysis.

Conclusions

In summary, we have successfully achieved precise control of the coordination environment around catalytic Ni^{2+} sites in COFs through a remote functionalization strategy. By altering the linkage from imine to β-ketoenamine linkage, we have realized the significantly improved activity, selectivity, and stability in the photocatalytic CO_2 reduction. Comprehensive experiments and theoretical calculations revealed that NiPor-BDOB exhibited exceptional photocatalytic performance, which originated from the effective suppression of electron–hole recombination, modulation of the electronic structure of Ni^{2+} sites, faster charge transfer in NiPor-BDOB, and optimized energy pathways in the CO_2 photoreduction process. This study introduced a simple and

DOI: 10.31635/ccschem.023.202303319
Citation: *CCS Chem.* **2024**, 6, 1689–1697
Link to VoR: https://doi.org/10.31635/ccschem.023.202303319

effective approach to precisely adjust the coordination environment surrounding catalytic metal sites, shedding light on the crucial interplay between the coordination microenvironment and catalysis.

Supporting Information

Supporting Information is available and includes materials and equipment detailed experimental procedures, characterizations, additional Figures S1–S17, Schemes S1 and S2, and Tables S1–S5.

Conflict of Interest

The authors declare no competing interests.

Funding Information

This work was supported by the National Key Research and Development Program of China (grant no. 2021YFA1500402), Strategic Priority Research Program of the Chinese Academy of Science (CAS; grant no. XDB0450302), National Natural Science Foundation of China (grant nos. U22A20401, 22161142001, and 22205224), China Postdoctoral Science Foundation (grant nos. BX2021281 and 2021M703064), and Fundamental Research Funds for the Central Universities (grant nos. WK2060000041 and WK3450000007).

References

1. Schneider, J.; Jia, H.; Muckerman, J. T.; Fujita, E. Thermodynamics and Kinetics of CO_2, CO, and H^+ Binding to the Metal Centre of CO_2 Reduction Catalysts. *Chem. Soc. Rev.* **2012**, *41*, 2036–2051.
2. Izumi, Y. Recent Advances in the Photocatalytic Conversion of Carbon Dioxide to Fuels with Water and/or Hydrogen Using Solar Energy and Beyond. *Coord. Chem. Rev.* **2013**, *257*, 171–186.
3. Hagfeldt, A.; Grätzel, M. Molecular Photovoltaics. *Acc. Chem. Res.* **2000**, *33*, 269–277.
4. Sato, S.; Arai, T.; Morikawa, T.; Uemura, K.; Suzuki, T. M.; Tanaka, H.; Kajino, T. Selective CO_2 Conversion to Formate Conjugated with H_2O Oxidation Utilizing Semiconductor/Complex Hybrid Photocatalysts. *J. Am. Chem. Soc.* **2011**, *133*, 15240–15243.
5. Inoue, T.; Fujishima, A.; Konishi, S.; Honda, K. Photoelectrocatalytic Reduction of Carbon Dioxide in Aqueous Suspensions of Semiconductor Powders. *Nature* **1979**, *277*, 637–638.
6. Xia, C.; Kirlikovali, K. O.; Nguyen, T. H. C.; Nguyen, X. C.; Tran, Q. B.; Duong, M. K.; Nguyen Dinh, M. T.; Nguyen, D. L. T.; Singh, P.; Raizada, P.; Nguyen, V.-H.; Kim, S. Y.; Singh, L.; Nguyen, C. C.; Shokouhimehr, M.; Le, Q. V. The Emerging Covalent Organic Frameworks (COFs) for Solar-Driven Fuels Production. *Coord. Chem. Rev.* **2021**, *446*, 214117.
7. Ran, J.; Jaroniec, M.; Qiao, S.-Z. Cocatalysts in Semiconductor-Based Photocatalytic CO_2 Reduction: Achievements, Challenges, and Opportunities. *Adv. Mater.* **2018**, *30*, 1704649.
8. Zhuo, T.-C.; Song, Y.; Zhuang, G.-L.; Chang, L.-P.; Yao, S.; Zhang, W.; Wang, Y.; Wang, P.; Lin, W.; Lu, T.-B.; Zhang, Z.-M. H-Bond-Mediated Selectivity Control of Formate Versus CO During CO_2 Photoreduction with Two Cooperative Cu/X Sites. *J. Am. Chem. Soc.* **2021**, *143*, 6114–6122.
9. Han, S.-G.; Zhang, M.; Fu, Z.-H.; Zheng, L.; Ma, D.-D.; Wu, X.-T.; Zhu, Q.-L. Enzyme-Inspired Microenvironment Engineering of a Single-Molecular Heterojunction for Promoting Concerted Electrochemical CO_2 Reduction. *Adv. Mater.* **2022**, *34*, 2202830.
10. Zhao, Y.; Hao, L.; Ozden, A.; Liu, S.; Miao, R. K.; Ou, P.; Alkayyali, T.; Zhang, S.; Ning, J.; Liang, Y.; Xu, Y.; Fan, M.; Chen, Y.; Huang, J. E.; Xie, K.; Zhang, J.; O'Brien, C. P.; Li, F.; Sargent, E. H.; Sinton, D. Conversion of CO_2 to Multicarbon Products in Strong Acid by Controlling the Catalyst Microenvironment. *Nat. Synth.* **2023**, *2*, 403–412.
11. Wang, J.; Sun, K.; Wang, D.; Niu, X.; Lin, Z.; Wang, S.; Yang, W.; Huang, J.; Jiang, H.-L. Precise Regulation of the Coordination Environment of Single Co(II) Sites in a Metal–Organic Framework for Boosting CO_2 Photoreduction. *ACS Catal.* **2023**, *13*, 8760–8769.
12. Huang, N.; Wang, P.; Jiang, D. Covalent Organic Frameworks: A Materials Platform for Structural and Functional Designs. *Nat. Rev. Mater.* **2016**, *1*, 16068.
13. Wei, P.-F.; Qi, M.-Z.; Wang, Z.-P.; Ding, S.-Y.; Yu, W.; Liu, Q.; Wang, L.-K.; Wang, H.-Z.; An, W.-K.; Wang, W. Benzoxazole-Linked Ultrastable Covalent Organic Frameworks for Photocatalysis. *J. Am. Chem. Soc.* **2018**, *140*, 4623–4631.
14. Kang, X.; Wu, X.; Han, X.; Yuan, C.; Liu, Y.; Cui, Y. Rational Synthesis of Interpenetrated 3D Covalent Organic Frameworks for Asymmetric Photocatalysis. *Chem. Sci.* **2020**, *11*, 1494–1502.
15. Chen, R.; Wang, Y.; Ma, Y.; Mal, A.; Gao, X.-Y.; Gao, L.; Qiao, L.; Li, X.-B.; Wu, L.-Z.; Wang, C. Rational Design of Isostructural 2D Porphyrin-Based Covalent Organic Frameworks for Tunable Photocatalytic Hydrogen Evolution. *Nat. Commun.* **2021**, *12*, 1354.
16. Fu, Z.; Wang, X.; Gardner, A. M.; Wang, X.; Chong, S. Y.; Neri, G.; Cowan, A. J.; Liu, L.; Li, X.; Vogel, A. A Stable Covalent Organic Framework for Photocatalytic Carbon Dioxide Reduction. *Chem. Sci.* **2020**, *11*, 543–550.
17. Lu, M.; Li, Q.; Liu, J.; Zhang, F.-M.; Zhang, L.; Wang, J.-L.; Kang, Z.-H.; Lan, Y.-Q. Installing Earth-Abundant Metal Active Centers to Covalent Organic Frameworks for Efficient Heterogeneous Photocatalytic CO_2 Reduction. *Appl. Catal. B Environ.* **2019**, *254*, 624–633.
18. Zhang, M.; Lu, M.; Lang, Z.-L.; Liu, J.; Liu, M.; Chang, J.-N.; Li, L.-Y.; Shang, L.-J.; Wang, M.; Li, S.-L. L.; Lan, Y.-Q. Semiconductor/Covalent-Organic-Framework Z-Scheme Heterojunctions for Artificial Photosynthesis. *Angew. Chem. Int. Ed.* **2020**, *59*, 6500–6506.
19. Zhong, W.; Sa, R.; Li, L.; He, Y.; Li, L.; Bi, J.; Zhuang, Z.; Yu, Y.; Zou, Z. A Covalent Organic Framework Bearing Single Ni Sites as a Synergistic Photocatalyst for Selective

DOI: 10.31635/ccschem.023.202303319
Citation: *CCS Chem.* **2024**, 6, 1689–1697
Link to VoR: https://doi.org/10.31635/ccschem.023.202303319

Photoreduction of CO_2 to CO. *J. Am. Chem. Soc.* **2019**, *141*, 7615–7621.
20. Wang, K.; Kang, X.; Yuan, C.; Han, X.; Liu, Y.; Cui, Y. Porous 2D and 3D Covalent Organic Frameworks with Dimensionality-Dependent Photocatalytic Activity in Promoting Radical Ring-Opening Polymerization. *Angew. Chem. Int. Ed.* **2021**, *60*, 19466–19476.
21. Meng, Y.; Luo, Y.; Shi, J.-L.; Ding, H.; Lang, X.; Chen, W.; Zheng, A.; Sun, J.; Wang, C. 2D and 3D Porphyrinic Covalent Organic Frameworks: The Influence of Dimensionality on Functionality. *Angew. Chem. Int. Ed.* **2020**, *59*, 3624–3629.
22. Zhi, Q.; Liu, W.; Jiang, R.; Zhan, X.; Jin, Y.; Chen, X.; Yang, X.; Wang, K.; Cao, W.; Qi, D.; Jiang, J. Piperazine-Linked Metalphthalocyanine Frameworks for Highly Efficient Visible-Light-Driven H_2O_2 Photosynthesis. *J. Am. Chem. Soc.* **2022**, *144*, 21328–21336.
23. Liu, M.; Jiang, K.; Ding, X.; Wang, S.; Zhang, C.; Liu, J.; Zhan, Z.; Cheng, G.; Li, B.; Chen, H.; Jin, S.; Tan, B. Controlling Monomer Feeding Rate to Achieve Highly Crystalline Covalent Triazine Frameworks. *Adv. Mater.* **2019**, *31*, 1807865.
24. Lu, M.; Zhang, M.; Liu, J.; Yu, T.-Y.; Chang, J.-N.; Shang, L.-J.; Li, S.-L. L.; Lan, Y.-Q. Confining and Highly Dispersing Single Polyoxometalate Clusters in Covalent Organic Frameworks by Covalent Linkages for CO_2 Photoreduction. *J. Am. Chem. Soc.* **2022**, *144*, 1861–1871.
25. Qian, Y.; Li, D.; Han, Y.; Jiang, H.-L. Photocatalytic Molecular Oxygen Activation by Regulating Excitonic Effects in Covalent Organic Frameworks. *J. Am. Chem. Soc.* **2020**, *142*, 20763–20771.
26. Zhao, Z.; Zheng, Y.; Wang, C.; Zhang, S.; Song, J.; Li, Y.; Ma, S.; Cheng, P.; Zhang, Z.; Chen, Y. Fabrication of Robust Covalent Organic Frameworks for Enhanced Visible-Light-Driven H_2 Evolution. *ACS Catal.* **2021**, *11*, 2098–2107.
27. Xu, X.; Cai, P.; Chen, H.; Zhou, H.-C.; Huang, N. Three-Dimensional Covalent Organic Frameworks with She Topology. *J. Am. Chem. Soc.* **2022**, *144*, 18511–18517.
28. Das, P.; Chakraborty, G.; Roeser, J.; Vogl, S.; Rabeah, J.; Thomas, A. Integrating Bifunctionality and Chemical Stability in Covalent Organic Frameworks via One-Pot Multicomponent Reactions for Solar-Driven H_2O_2 Production. *J. Am. Chem. Soc.* **2023**, *145*, 2975–2984.
29. Lin, G.; Ding, H.; Chen, R.; Peng, Z.; Wang, B.; Wang, C. 3D Porphyrin-Based Covalent Organic Frameworks. *J. Am. Chem. Soc.* **2017**, *139*, 8705–8709.
30. Liang, R.-R.; Xu, S.-Q.; Zhang, L.; A, R.-H.; Chen, P.; Cui, F.-Z.; Qi, Q.-Y.; Sun, J.; Zhao, X. Rational Design of Crystalline Two-Dimensional Frameworks with Highly Complicated Topological Structures. *Nat. Commun.* **2019**, *10*, 4609.
31. Wang, J.; Zhu, W.; Meng, F.; Bai, G.; Zhang, Q.; Lan, X. Integrating Dual-Metal Sites Into Covalent Organic Frameworks for Enhanced Photocatalytic CO_2 Reduction. *ACS Catal.* **2023**, *13*, 4316–4329.
32. Lin, S.; Diercks, C. S.; Zhang, Y.-B.; Kornienko, N.; Nichols, E. M.; Zhao, Y.; Paris, A. R.; Kim, D.; Yang, P.; Yaghi, O. M.; Chang, C. J. Covalent Organic Frameworks Comprising Cobalt Porphyrins for Catalytic CO_2 Reduction in Water. *Science* **2015**, *349*, 1208–1213.
33. Diercks, C. S.; Lin, S.; Kornienko, N.; Kapustin, E. A.; Nichols, E. M.; Zhu, C.; Zhao, Y.; Chang, C. J.; Yaghi, O. M. Reticular Electronic Tuning of Porphyrin Active Sites in Covalent Organic Frameworks for Electrocatalytic Carbon Dioxide Reduction. *J. Am. Chem. Soc.* **2018**, *140*, 1116–1122.
34. Liu, Y.; Wang, Y.; Li, H.; Guan, X.; Zhu, L.; Xue, M.; Yan, Y.; Valtchev, V.; Qiu, S.; Fang, Q. Ambient Aqueous-Phase Synthesis of Covalent Organic Frameworks for Degradation of Organic Pollutants. *Chem. Sci.* **2019**, *10*, 10815–10820.
35. Wan, S.; Gándara, F.; Asano, A.; Furukawa, H.; Saeki, A.; Dey, S. K.; Liao, L.; Ambrogio, M. W.; Botros, Y. Y.; Duan, X.; Seki, S.; Stoddart, J. F.; Yaghi, O. M. Covalent Organic Frameworks with High Charge Carrier Mobility. *Chem. Mater.* **2011**, *23*, 4094–4097.
36. Wang, H.; Qian, C.; Liu, J.; Zeng, Y.; Wang, D.; Zhou, W.; Gu, L.; Wu, H.; Liu, G.; Zhao, Y. Integrating Suitable Linkage of Covalent Organic Frameworks into Covalently Bridged Inorganic/Organic Hybrids Toward Efficient Photocatalysis. *J. Am. Chem. Soc.* **2020**, *142*, 4862–4871.
37. Lu, M.; Liu, J.; Li, Q.; Zhang, M.; Liu, M.; Wang, J.-L.; Yuan, D.-Q.; Lan, Y.-Q. Rational Design of Crystalline Covalent Organic Frameworks for Efficient CO_2 Photoreduction with H_2O. *Angew. Chem. Int. Ed.* **2019**, *58*, 12392–12397.
38. Wu, Q.-J.; Liang, J.; Huang, Y.-B.; Cao, R. Thermo-, Electro-, and Photocatalytic CO_2 Conversion to Value-Added Products Over Porous Metal/Covalent Organic Frameworks. *Acc. Chem. Res.* **2022**, *55*, 2978–2997.
39. Liu, X.; Yang, Y.; Chen, M.; Xu, W.; Chen, K.; Luo, R. High-Surface-Area Metalloporphyrin-Based Porous Ionic Polymers by the Direct Condensation Strategy for Enhanced CO_2 Capture and Catalytic Conversion into Cyclic Carbonates. *ACS Appl. Mater. Interfaces* **2023**, *15*, 1085–1096.
40. Zhou, W.; Deng, Q.-W.; Ren, G.-Q.; Sun, L.; Yang, L.; Li, Y.-M.; Zhai, D.; Zhou, Y.-H.; Deng, W.-Q. Enhanced Carbon Dioxide Conversion at Ambient Conditions via a Pore Enrichment Effect. *Nat. Commun.* **2020**, *11*, 4481.
41. Zou, Z.; Ye, J.; Sayama, K.; Arakawa, H. Direct Splitting of Water Under Visible Light Irradiation with an Oxide Semiconductor Photocatalyst. *Nature* **2001**, *414*, 625–627.
42. Wang, X.; Maeda, K.; Thomas, A.; Takanabe, K.; Xin, G.; Carlsson, J. M.; Domen, K.; Antonietti, M. A Metal-Free Polymeric Photocatalyst for Hydrogen Production from Water Under Visible Light. *Nat. Mater.* **2009**, *8*, 76–80.
43. Chi, X.; Lan, Z.-A.; Chen, Q.; Zhang, X.; Chen, X.; Zhang, G.; Wang, X. Electronic Transmission Channels Promoting Charge Separation of Conjugated Polymers for Photocatalytic CO_2 Reduction with Controllable Selectivity. *Angew. Chem. Int. Ed.* **2023**, *62*, e202303785.
44. Zhou, C.; Wang, S.; Zhao, Z.; Shi, Z.; Yan, S.; Zou, Z. A Facet-Dependent Schottky-Junction Electron Shuttle in a $BiVO_4${010}–Au–Cu_2O Z-Scheme Photocatalyst for Efficient Charge Separation. *Adv. Funct. Mater.* **2018**, *28*, 1801214.

DOI: 10.31635/ccschem.023.202303319
Citation: *CCS Chem.* **2024**, 6, 1689–1697
Link to VoR: https://doi.org/10.31635/ccschem.023.202303319